Supporting information for

pH Dependent Electronic and Geometric Structures at the Water-Silica Nanoparticle Interface

Matthew A. Brown,[a]* Marco Arrigoni,[b] Florent Héroguel,[c] Amaia Beloqui Redondo,[a]
Livia Giordano,[b] Jeroen A. van Bokhoven,[a,d] and Gianfranco Pacchioni[b]*

a) Institute for Chemical and Bioengineering, ETH Zürich, CH-8093 Zurich, Switzerland
b) Dipartimento di Scienza dei Materiali, Università di Milano-Bicocca, 20125 Milan, Italy
c) Laboratory of Inorganic Chemistry, ETH Zürich, CH-8093 Zurich, Switzerland
d) Paul Scherrer Institute, CH-5232 Villigen PSI, Switzerland

E-Mail: matthew.brown@chem.ethz.ch (M.A.B.) and gianfranco.pacchioni@unimib.it (G.P.)

X-ray Photoelectron Spectroscopy (XPS)

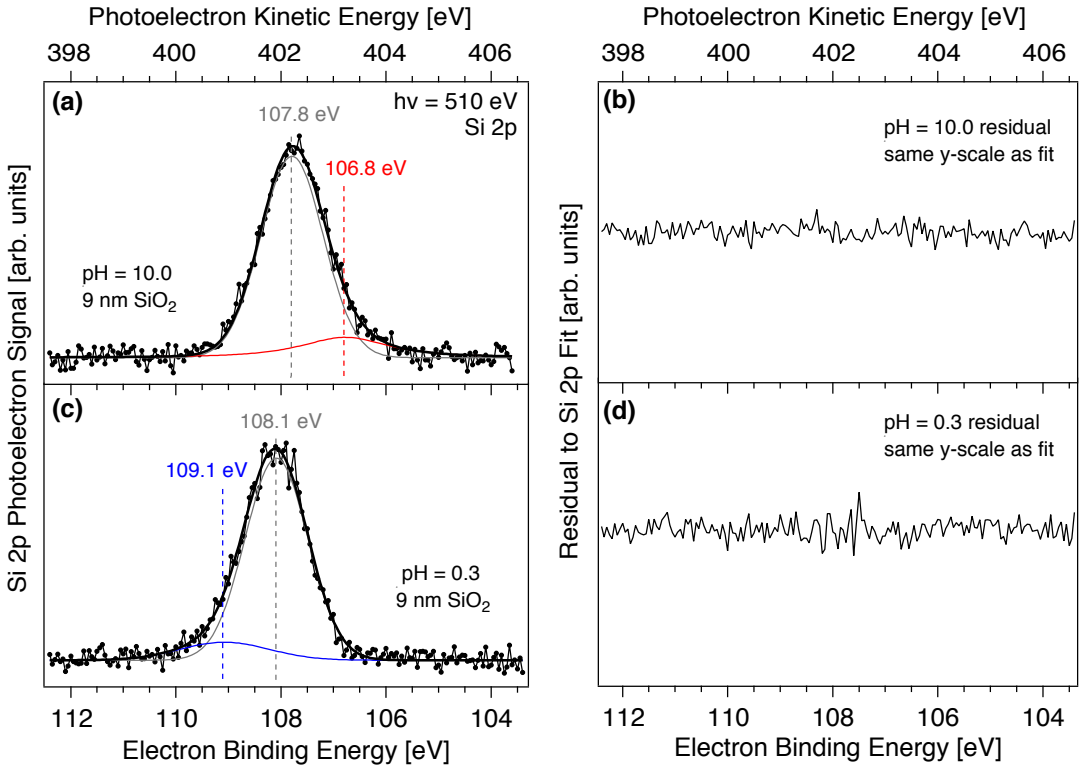

Figure S1. Silicon 2p spectra collected at (a) pH 10.0 and (c) pH 0.3 from a liquid microjet of 10 wt % 9 nm colloidal SiO_2. Both spectra are fit using two Gaussian functions. The residuals to the fit are shown in (b) and (c). At high pH the shoulder component is on the low BE size of the main peak, whereas at low pH the shoulder is on the high BE side. The electron binding energy scale is relative to the vacuum level.

Figure S2 shows the O 1s XP spectra recorded from a liquid microjet of a 10 wt % suspension of 9 nm SiO_2 at pH 10.0 (red), and from a solution of water that contains 0.05 M NaCl (blue) as a silica-free reference solution, which allows for the shape and BE of the O 1s signal from the water solvent to be determined, Table 1. The O 1s spectra were collected with an incident photon energy of 930 eV, which corresponds to a pKE of ca. 392 eV. Collecting the Si 2p and O 1s spectra regions with similar pKE ensures the same probe depth of the experiment. Both O 1s spectra have a single intense component centered at a BE

of 538.1 eV and with a fwhm of 1.8 eV that is characteristic of liquid water.[1] The difference of the two O 1s spectra represents the contribution to the O 1s region from the silica NPs. The difference spectrum is shown in black in Figure S2. It is clear that no contribution from the silica NPs is evident in the spectrum. For reference the expected positions of the O 1s component from silica, based on the energy difference between the O 1s and Si 2p regions taken from silica samples in vacuum[2, 3] and added to the 108.1-107.8 eV BE we measured in the Si 2p spectra (Figure S1a, S1c), is included in Figure S2. The difference in BE between the O 1s components of liquid water and the expected position in silica is only 0.2-0.8 eV, and prevents the silica contribution from being detected above the relatively strong signal produced by the water solvent. No O 1s spectral contribution is observed for the silica suspension at pH 0.3 (not shown).

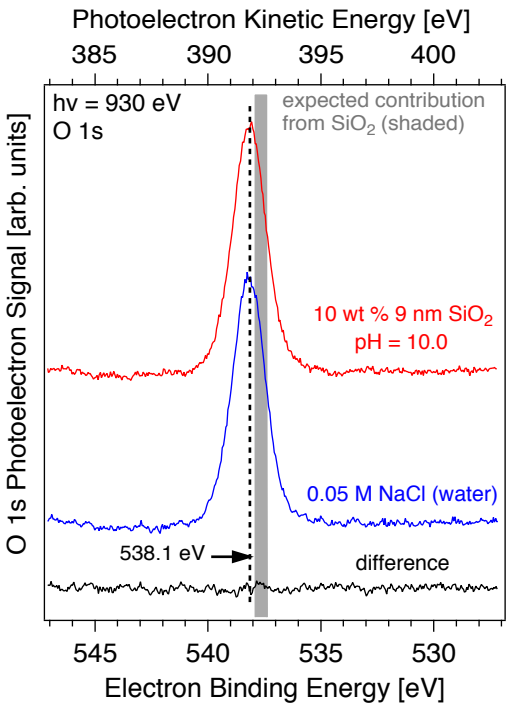

Figure S2. Oxygen 1s spectra from a 10 wt % suspension of SiO_2 at pH 10.0 (red, top) and from an aqueous solution of 0.05 M NaCl (blue, middle) that serves as a reference to the O 1s region. The difference spectrum (black, bottom) shows the contribution of the silica NPs to the O 1s region. For reference, the expected BE of the silica NPs is shown as a shaded bar. It is clear that no contribution to the O 1s spectrum can be attributed to the NPs. The electron binding energy scale is relative to the vacuum level.

The O 1s region of the XP spectra shows no distinct silica signal. The experiments were performed at 10 wt % silica, corresponding to 3 mol % SiO_2 (ca. 97 mol % H_2O) based on the 9 nm particles' volume. At a pKE of 400 eV the inelastic mean free path (IMFP) in silica is well known to be 1.76 nm,[4] and assuming the probe depth of the experiment is 3× the IMFP (here we are assuming that the IMFP in silica and liquid water are similar at 400 eV pKE) only 64 % of the particles' volume is available to be 'seen' by XPS. This is an upper bound as the particles are hydrophilic and believed to reside several molecular layers below the air-water interface,[5-8] which further suppresses their relative

signal intensity in an XPS experiment (i.e., water layers between the NP and the air-water interface attenuate the signal from the NP with an exponential dependence[9]). If the tops of the particles are 1 nm below the air-water interface the available XPS probe volume of the particles is reduced to 48 %, and to 31 % with 2 nm of water between the particles' surfaces and the air-water interface.[9] If we conservatively estimate,[8] based on the hydrophilic character of charge-stabilized silica, that the particles are 3 molecular layers of water below the air-water interface (ca. 0.9 nm), approximately half of the particles' volume is available for XPS. This reduces the relative silica concentration to 1.5 mol %. While a 1.5 mol % concentration should normally be detected in an XPS experiment, and it is for the Si 2p region for which the same concentration arguments hold (although with a BE of only 108 eV we gain in the Si 2p region by being able to use a photon energy with a higher flux) the O 1s region is further complicated by the strong signal from the solvent water and the near spectral overlap of the two components (Figure S2). All of these factors taken together, and no spectral signature from the NPs can be detected in the O 1s region.

Nuclear Magnetic Resonance (NMR)

Table S1. Summary of the measured NMR chemical shift (ppm), full width half maximum (FWHM), and relative signal intensity for thick gel-like 9 nm SiO_2 suspensions (results from Figure 5).

	δ(^{29}Si) ppm	fwhm ppm	Relative intensity %
pH 10.0			
Q_4	−111	9.0	72
Q_3	−101	7.4	23
Q_2	−91	6.3	5
pH 6.5			
Q_4	−112	9.1	79
Q_3	−101	7.0	17
Q_2	−92	6.6	4
pH 4.0			
Q_4	−112	8.5	72
Q_3	−102	6.5	23
Q_2	−92	6.4	5
pH 1.0			
Q_4	−112	8.7	67
Q_3	−101	6.2	27
Q_2	−91	5.8	6
pH 0.1			
Q_4	−112	8.5	66
Q_3	−102	6.4	28
Q_2	−92	5.9	6

Study of the chemical shift anisotropy (observation of spinning side bands). While the various surface species could not be distinguished by SP ^{29}Si NMR, their chemical shift anisotropy parameters are significantly different as determined by calculations. We hence investigated the acquisition of ^{29}Si NMR spectra at various spinning rates in order to observe the spinning side bands positions to fit chemical shift anisotropy parameters. Unfortunately, only one spinning side bands was observed upfield, while a minimum of 3 spinning side bands are required for a reliable curve fitting and thus reliable information

concerning chemical shift anisotropy. The only conclusion is that Q_4 silicon have a positive skew as the spinning side band was observed upfield.

In Table S2 we report the computed NMR properties for the various silanol centers discussed in the paper. The values have been obtained using Model 1 of silica nanoparticles (see text).

Table S2. NMR properties computed for various groups in silica nano-clusters (Model 1): isotropic schielding, $\sigma_{iso}(^{29}Si)$; chemical shift, $\delta(^{29}Si)$; span, Ω; Skew, κ; quadrupolar coupling, $C_Q(^{17}O)$; asymmetry parameter, $\eta_Q(^{17}O)$

		$\sigma_{iso}(^{29}Si)$ ppm	$\delta(^{29}Si)$[a] ppm	Ω ppm	κ	$C_Q(^{17}O)$ MHz	$\eta_Q(^{17}O)$
≡Si=	Q_4	445	–117	43	0.4	-	-
≡Si-OH	Q_3	433	–106	60±13	0.5±0.2	–8.0±0.1	0.6
=Si(OH)$_2$	Q_2	423	–95	52±15	0.0±0.1	-	-
≡Si-O$^-$	Q_3	438	–110	200	0.9	–2.5	0.1
≡Si-OH$_2^+$	Q_3	435	–107	85	–0.4	10.6	0.3
=SiOH(OH$_2^+$)	Q_3	428	-100	109	-0.4		
≡Si-O-Si≡	-	-	-	-	-	–5.9±0.2[b]	0.2±0.1[b]

a) Reference value for TMS $\sigma_{iso}(^{29}Si)$ = 328 ppm

b) Experimental values: C_Q = –5.2±0.1; η_Q = 0.292±0.005[10]

^1H-^{29}Si cross polarization dynamics study

INTRODUCTION

The natural isotopic abundance of the half spin nucleus ^{29}Si is relatively low (4.69%). As too is its gyromagnetic ratio (–53.2 . 10^6 rad.s^{-1}.T^{-1}), which leads to low sensitivity compared to ^1H NMR. To overcome this issue, silicon atoms can benefit from the high sensitivity of surrounding protons thanks to the cross-polarization (CP) technique:[11] ^1H are first polarized, the polarization is then transferred from ^1H to ^{29}Si and the signal is detected on ^{29}Si. The CP technique is not quantitative as the polarization enhancement of a silicon atom depends of the proximity of protons and of the efficiency of the polarization transfer. While

the latter fact could appear as a drawback of the CP technique, important information can be obtained by studying CP dynamics. In silica, cross-polarization is more efficient for silicons from silanol (Q_3 and Q_2) than for bulk silicons (Q_4) due to the Si-H proximity for the former. For short CP contact times (below 1 ms), silanol would be enhanced while this delay is not sufficient for spin diffusion to bulk silicons. Increasing the CP contact time can increase the efficiency of the cross polarization up to a certain maximum, after which further increasing the contact time results in a decrease due to spin relaxation. For silanol, this maximum will be reached for a relatively short CP contact time while the maximum for bulk silicon will be reached for longer CP contact time. The evolution of the magnetization, and thus the intensity, regarding the CP contact time follows the equation:[12, 13]

$$M(t) = \frac{M^{\infty}}{1 - \frac{T_{SiH}}{T_{1\rho,H}}}\left[\exp\left(\frac{-t}{T_{1\rho,H}}\right) - \exp\left(\frac{-t}{T_{SiH}}\right)\right] \qquad \text{(S1)}$$

where T_{SiH} is the H-Si cross-polarization time constant and $T_{1\rho,H}$ is the proton spin-lattice relaxation time. A strong ^{1}H - ^{29}Si dipolar interaction means a small T_{SiH} value. Direct relaxation of silicon is extremely slow compared to proton ($T_{1\rho,Si} >> T_{1\rho,H}$) so relaxation occurs via surrounding protons, and thus the exponential decay of eq. 1 has the constant $T_{1\rho,H}$.

The surface characterization of silica gels by analysis of cross polarization relaxation parameters was investigated as early as 1971 by Maciel *et al.*,[14] while this approach was applied more recently to characterize the surface of fumed silica.[12] Comparison of low or high surfaces areas silica gels was achieved by

study of the influence of silanol deuteration on CP efficiency.[15] Combination of ssNMR and chemometrics was used to probe the sorption behavior of paramagnetic cations at the amorphous silica surface, where the coordination of a cation on a deprotonated silanol decreases the efficiency of the cross-polarization between silanol protons and silicon atoms from deprotonated silanols where cation is sorbed.[16]

RESULTS AND DISCUSSION

We studied cross polarization dynamics by variable contact time experiment at two pH, 1.0 and 10.0, for contact times varying from 1 to 15 ms (spectra for longer CP contact time were not recorded as a high power delivered for times longer than 15 ms could damage the NMR probe). One can note that while Q_2 sites were clearly observed in ^{29}Si SP MAS NMR at –90 ppm, only a small shoulder was observed by ^{29}Si CP MAS (Figures S3 and S4). Spectra were decomposed and the area of Q_3 (−100 ppm) and Q_4 (−110 ppm) peaks were plotted in respect to contact time (Figure S5). For both samples, intensity of Q_4 increases relatively slowly with increasing contact time, as expected because of the absence of neighboring protons for bulk silicon atoms. We can note that while Q_4 peaks were larger than Q_3 for SP experiment, the relative intensity of Q_4 is decreased with CP as polarization transfer is less efficient for bulk silicon, and is most likely limited to one or two layers of silicon below the surface. In both samples, the exponential decay due to spin-lattice relaxation was not observed in the time domain of the experiment and so assumed to be superior to 30 ms. Hence, we approximate $\frac{T_{SiH}}{T_{1\rho,H}} \approx 0$ and the intensity follows the equation:

$$M(t) = M^{\infty}\left[1 - \exp\left(\frac{-t}{T_{SiH}}\right)\right] \qquad \text{(S2)}$$

As expected, values obtained from data fitting (presented in Table S3) gave relatively large values of T_{SiH} (12.8 and 14.4 ms for pH = 1 and 10 samples respectively) as the Q_4 sites are not directly bonded to protons. We should note that this exponential decay differs from a recent study reporting a square root behavior due to spin diffusion.[16] Q_3 sites for low pH sample present a similar behavior where the decay is not observed, but with a faster growth (T_{SiH} = 2.8 ms) in agreement with a close proximity of protons at the surface. Finally, Q_3 sites from high pH (fitted with the bi-exponential model of eq. S1) present a fast growth of intensity (T_{SiH} = 2 ms) comparable to Q_3 from low pH sample but a relatively fast decay as well ($T_{1\rho,H}$ =18 ms). In opposition to the higher value for low pH sample, we propose that this relatively fast relaxation occurs *via* sodium cations, which are strongly interacting with the negatively charged surface at high pH but away from the positively charged surface at low pH. In fact, ^{29}Si relaxation *via* ^{23}Na was observed in polycrystalline sodium salt of adenosine monophosphate.[17] The quadrupolar nuclei (spin 3/2) ^{23}Na have a 100% isotopic natural abundance and electric quadrupolar relaxation is very efficient as quadrupolar nuclei are characterized by a non-spherical distribution of electric charges and possess an electric magnetic moment (Q_{23Na} = 10.4 . 10^{-28} m^2). This mechanism dominates over relaxation through protons via dipole–dipole interaction as the latter phenomena is limited because of relatively high Si-H distance. While we propose here an indirect ^{29}Si relaxation favored by the

proximity of sodium, we exclude direct scalar relaxation between ^{29}Si and ^{23}Na, as frequencies of the latter do no match (105.842 MHz for ^{23}Na vs 79.495 MHz for ^{29}Si at 9.40 T). This fast relaxation through sodium is not observed at low pH as sodium cations and chlorine anions (which present 2 quadrupolar nucleus ^{35}Cl and ^{37}Cl) are most probably not strongly interacting with the surface pH due to the high proton density on the latter.

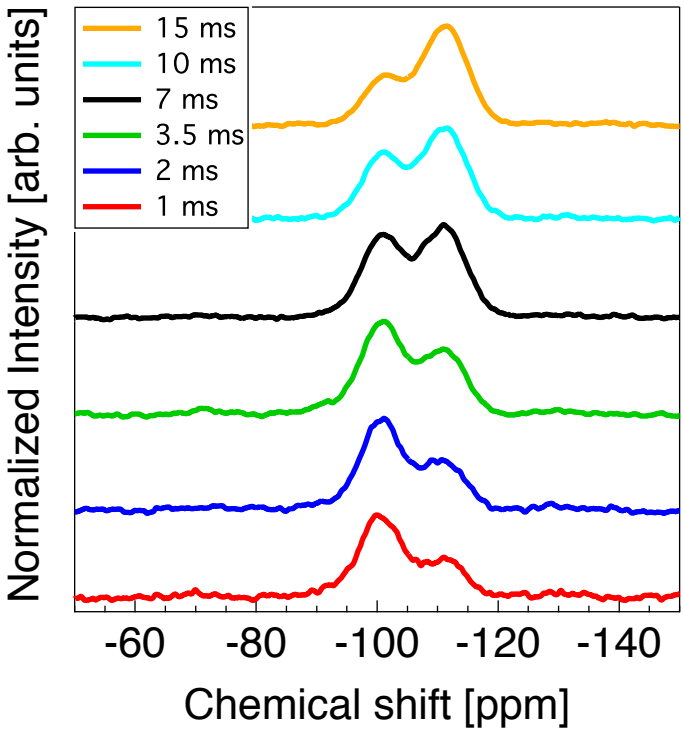

Figure S3: ^{1}H-^{29}Si CP MAS NMR spectra of dried silica solutions at pH 10.0 (offset for clarity in the y axis).

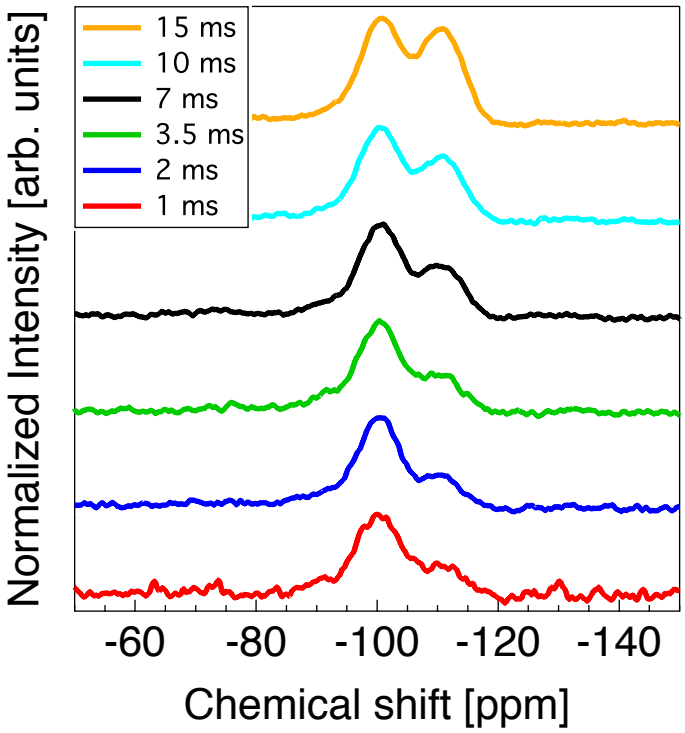

Figure S4: ^{1}H-^{29}Si CP MAS NMR spectra of dried silica solutions at pH 1.0 (offset for clarity in the y axis).

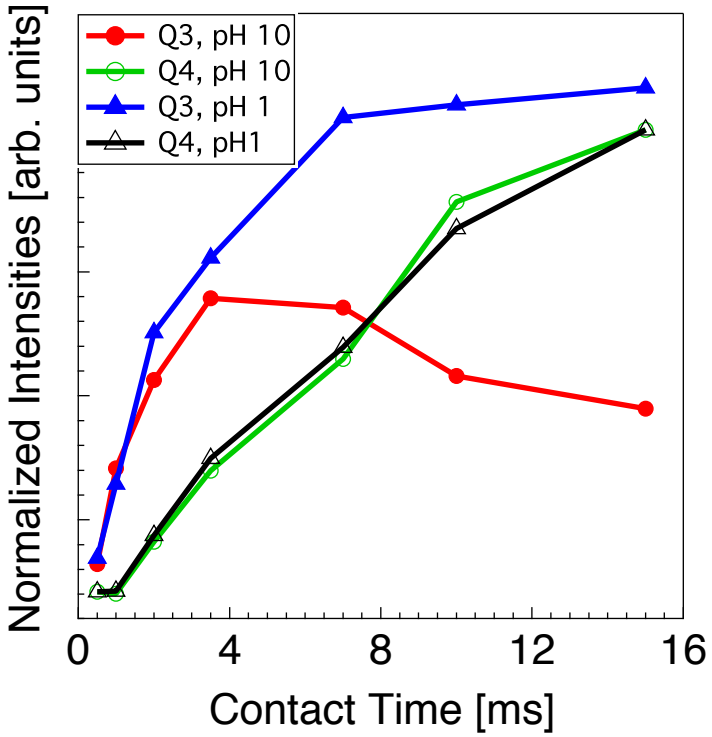

Figure S5: Area of Q_3 (−100 ppm) and Q_4 (−110 ppm) peaks versus contact time after decomposition for dried silica solutions at pH 10.0 and pH 1.0.

Table S3. H-Si cross-polarization time constants (T_{SiH}) and proton spin-lattice relaxation times ($T_{1\rho,H}$) for Q_3 and Q_4 sites at pH 1.0 and 10.0, as determined by fitting the intensities of the respective peaks for various contact times with equations 1 or 2.

pH	site	T_{SiH} (ms)	$T_{1\rho,H}$ (ms)
1.0	Q_3	2.8	>30
	Q_4	12.8	>30
10.0	Q_3	2	18
	Q_4	14.4	>30

REFERENCES

1. Brown, M. A.; Winter, B.; Faubel, M.; Hemminger, J. C. Spatial Distributions of Nitrate and Nitrite Anions at the Liquid/Vapor Interface of Aqueous Solutions. *Journal of the American Chemical Society* 2009, 131, 8354-8355.
2. Bancroft, G. M.; Nesbitt, H. W.; Ho, R.; Shaw, D. M.; Tse, J. S.; Biesinger, M. C. Toward a Comprehensive Understanding of Solid-State Core-Level XPS Linewidths: Experimental and Theoretical Studies on the Si 2p and O 1s Linewidths in Silicates. *Phys Rev B* 2009, 80, 075405.

3. Gross, T.; Ramm, M.; Sonntag, H.; Unger, W.; Weijers, H. M.; Adem, E. H. An XPS Analysis of Different SiO2 Modifications Employing a C 1s as Well as an Au 4f7/2 Static Charge Reference. *Surf Interface Anal* 1992, 18, 59-64.
4. Powell, C. J.; Jablonski, A. *NIST Electron Inelastic-Mean-Free-Path Database*, Version 1.1; National Institute of Standards and Technology: Gaithersburg, MD, 2000.
5. Brown, M. A.; Duyckaerts, N.; Beloqui Redondo, A.; Jordan, I.; Nolting, F.; Kleibert, A.; Ammann, M.; Woerner, H. J.; van Bokhoven, J. A.; Abbas, Z. Effect of Surface Charge Density on the Affinity of Oxide Nanoparticles for the Vapor-Water Interface. *Langmuir* 2013, 29, 5023-5029.
6. Blute, I.; Pugh, R. J.; van de Pas, J.; Callaghan, I. Industrial Manufactured Silica Nanoparticle Sols. 2: Surface Tension, Particle Concentration, Foam Generation and Stability. *Colloid Surface A* 2009, 337, 127-135.
7. Ravera, F.; Santini, E.; Loglio, G.; Ferrari, M.; Liggieri, L. Effect of Nanoparticles on the Interfacial Properties of Liquid/Liquid and Liquid/Air Surface Layers. *J Phys Chem B* 2006, 110, 19543-19551.
8. Jordan, I.; Beloqui Redondo, A.; Brown, M. A.; Fodor, D.; Staniuk, M.; Kleibert, A.; Wörner, H. J.; Giorgi, J. B.; van Bokhoven, J. A. Non-Uniform Spatial Distribution of Tin Oxide (SnO2) Nanoparticles at the Air-Water Interface. *Chemical Communications* 2014, 50, 4242-4244.
9. Brown, M. A.; Jordan, I.; Beloqui Redondo, A.; Kleibert, A.; Wörner, H. J.; van Bokhoven, J. A. In Situ Photoelectron Spectroscopy at the Liquid/Nanoparticle Interface. *Surf Sci* 2013, 610, 1-6.
10. Grandinetti, P. J.; Baltisberger, J. H.; Farnan, I.; Stebbins, J. F.; Werner, U.; Pines, A. Solid-State O-17 Magic-Angle and Dynamic-Angle Spinning NMR-Study of the SiO_2 Polymorph Coesite. *Journal of Physical Chemistry* 1995, 99, 12341-12348.
11. Pines, A.; Gibby, M. G.; Waugh, J. S. Proton-Enhanced NMR of Dilute Spins in Solids. *J. Chem. Phys.* 1973, 59, 569-590.
12. Liu, C. H. C.; Maciel, G. E. The fumed silica surface: A study by NMR. *J. Am. Chem. Soc.* 1996, 118, 5103-5119.
13. Kolodziejski, W.; Klinowski, J. Kinetics of Cross-Polarization in Solid-State NMR: A Guide for Chemists. *Chem. Rev.* 2002, 102, 613-628.
14. Maciel, G. E.; Sindorf, D. W. Si-29 Nuclear Magnetic-Resonance Study of the Surface of Silica-Gel by Cross Polarization and Magic-Angle Spinning. *J. Am. Chem. Soc.* 1980, 102, 7606-7607.
15. Chuang, I. S.; Kinney, D. R.; Maciel, G. E. Interior Hydroxyls of the Silica-Gel System as Studied by Si-29 CP-MAS NMR-Spectroscopy. *J. Am. Chem. Soc.* 1993, 115, 8695-8705.
16. Mason, H. E.; Harley, S. J.; Maxwell, R. S.; Carroll, S. A. Probing the Surface Structure of Divalent Transition Metals Using Surface Specific Solid-State NMR Spectroscopy. *Environ. Sci. Technol.* 2012, 46, 2806-2812.
17. Reynhardt, E. C.; Froneman, S.; Andrew, E. R.; Szczesniak, E. An Nmr-Study of H-1, P-31, and Na-23 Relaxation and Molecular-Dynamics in the Polycrystalline Sodium-Salt of Adenosine-Monophosphate. *J. Magn. Reson.* 1989, 84, 110-120.